Research Letter DOI: 10.15541/jim20240136

Performance of Lateral 4H-SiC Photoconductive Semiconductor Switches by Extrinsic Backside Trigger

WANG Hao[1,2], LIU Xuechao[1], ZHENG Zhong[3], PAN Xiuhong[1], XU Jintao[1], ZHU Xinfeng[1,2], CHEN Kun[1], DENG Weijie[1], TANG Meibo[1], GUO Hui[3], GAO Pan[4]

(1. Shanghai Institute of Ceramics, Chinese Academy of Sciences, Shanghai 201889, China; 2. University of Chinese Academy of Sciences, Beijing 100049, China; 3. School of Microelectronics, Xidian University, Xi'an 710071, China; 4. School of Material Science, Shanghai Dianji University, Shanghai 201306, China)

Abstract: Photoconductive semiconductor switch (PCSS) can be applied in pulsed high power systems and microwave techniques. However, reducing the damage and increasing the lifetime of silicon carbide (SiC) PCSS are still faced severe challenges. In this study, PCSSs with various structures were prepared on 4-inch diameter, 500 μm thick high-purity semi-insulating 4H-SiC substrates and their on-state resistance and damage mechanisms were investigated. It was found that the PCSS of an Au/TiW/Ni electrode system annealed at 950 ℃ had a minimum on-state resistance of 6.0 Ω at 1 kV bias voltage with a 532 nm and 170 mJ pulsed laser by backside illumination single trigger. The backside illumination single trigger could reduce on-state resistance and alleviate the damage of PCSS compared to the frontside trigger when the diameter of the laser spot was larger than the channel length of PCSS. For the 200 s trigger test by a 10 Hz laser, the black branch-like ablation on Au/TiW/Ni PCSS was mainly caused by thermal stress owing to hot carriers. Replacing metal Ni with boron gallium co-doped zinc oxide (BGZO) thin films annealed at 400 ℃, black branch-like ablation was alleviated while concentric arc damage was obvious at the anode. The major causes of concentric arc are both pulsed laser diffraction and thermal effect.

Key words: silicon carbide; photoconductive semiconductor switch; on-state resistance; failure analysis

A photoconductive semiconductor switch (PCSS) can be on-state and off-state by using a pulsed laser to control the conductivity of a semi-insulting semiconductor[1]. PCSS can be applied in high-power microwave devices[2], dielectric wall accelerators[3], and terahertz technology[4-5]. PCSS has the advantages of compact geometry, lower jitter, faster rising and falling time, higher repetition frequency, and larger power capacity[6]. Gallium arsenide (GaAs) based PCSS can achieve high power in nonlinear mode and be triggered by low energy laser (nJ), but the withstand voltage of a single device is insufficient[7-8]. Silicon carbide (SiC) single crystal has the superior properties of wide bandgap (4H-SiC: ~3.26 eV), high critical breakdown field strength (~3 MV/cm), and high thermal conductivity (~3.7 W/(cm·K))[9]. Although SiC PCSS generally operates in linear mode, it can theoretically achieve higher output power and higher frequency operation compared to GaAs PCSS due to its high withstand voltage[10-11]. However, it is difficult to keep the balance between high power and long device lifetime, and research on the damage characteristics and mechanisms of SiC PCSS has not been clear yet[12-14]. Zhu *et al*.[15] introduced a highly n-doped gallium nitride (GaN) layer into SiC PCSS to alleviate the damage at the cathode of PCSS, which is caused by Joule heating. Xiao *et al*.[16] observed that cracks tended to occur at the anode of PCSS with GaN layer due to electron avalanche breakdown. Mauch *et al*.[17] investigated that the transient electric fields at the metal/SiC interface led to the degradation of lateral PCSS since the laser distribution was not uniform. Besides, transparent oxide conductive electrodes, such as aluminum-doped zinc

Received date: 2024-03-20; **Revised date:** 2024-04-10; **Published online:** 2024-04-19
Foundation item: National Key R&D Program of China (2021YFA0716304); Shanghai Science and Technology Programs (22511100300, 23DZ2201500)
Biography: WANG Hao (1999–), male, Master candidate. E-mail: wanghao218@mails.ucas.ac.cn
王 浩(1999–), 男, 硕士研究生. E-mail: wanghao218@mails.ucas.ac.cn
Corresponding author: LIU Xuechao, professor. E-mail: xcliu@mail.sic.ac.cn
刘学超, 研究员. E-mail: xcliu@mail.sic.ac.cn

oxide (AZO), were used to reduce PCSS on-state resistance[18-19]. Nevertheless, the ablation of AZO films by laser was prone to cracks[20]. The local temperature of SiC PCSS could rise to near 980 K when PCSS was on-state by stimulation[21]. These results show that the high electric field strength plays an important role in PCSS breakdown. The thermal effects cannot be ignored either, especially in multiple triggers and high-frequency operations. Therefore, to enhance withstand voltage and reduce on-state resistance, more research is needed on damage phenomena and failure mechanisms to guide PCSS design.

In this work, several lateral 4H-SiC PCSSs were made and tested by a 532 nm laser extrinsic trigger. The on-state resistance and damage phenomena of PCSSs by frontside illumination (FSI) single trigger, backside illumination (BSI) single trigger, and multiple triggers were investigated and discussed.

1　Experimental

1.1　Fabrication processes

The basic processes of fabricating lateral PCSSs on homemade 4-inch diameter high-purity semi-insulating (HPSI) 4H-SiC crystal substrates (0.5 mm thick) are shown in Fig. 1. Two kinds of SiC substrates were used (marked as SiC1 and SiC2). The substrates were cleaned with a sequence of standard RCA cleaning. The metal electrode patterns were formed by photolithography, magnetron sputtering, and lift-off process. Au, TiW, Ni, and boron and gallium co-doped zinc oxide (BGZO) layers were deposited by sputtering. The BGZO target consists (in mass) of 0.5% boron oxide, 2.5% gallium, and 97% zinc oxide. The 12 mm×12 mm PCSS samples were obtained from substrates by dicing before annealing. As shown in Fig. 2(a, b), two types of PCSS samples with Au/TiW/Ni and Au/TiW/BGZO electrodes

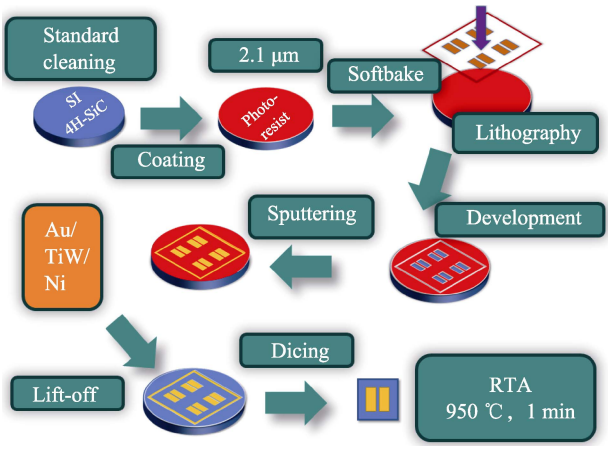

Fig. 1　Basic fabrication flowchart of SiC PCSS

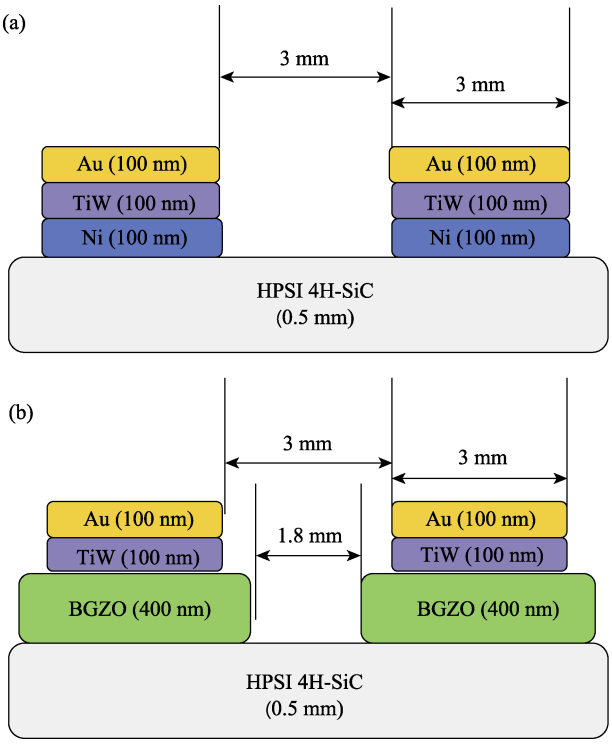

Fig. 2　Diagrams of SiC PCSS electrodes components
(a) Au/TiW/Ni/SiC; (b) Au/TiW/BGZO/SiC

components were designed, marked as SiC_Ni PCSS and SiC_BGZO PCSS. For SiC_Ni PCSS samples, each of the metal was deposited for 100 nm. The distance between the two electrodes (channel length) was 3 mm. Ohmic contacts of SiC_Ni PCSS samples were formed by rapid thermal anneal (RTA) at 950 ℃ for 1 min. For SiC_BGZO PCSS, 400 nm BGZO films were deposited instead of Ni and the distance was 1.8 mm. SiC_BGZO PCSS samples were annealed at 400 ℃ for 30 min in Ar ambient and cooled down in a tube furnace.

1.2　Test methods

The PCSS test circuit diagram is shown in Fig. 3. PCSSs were triggered by Nd:YAG solid-state laser (Dawa-300). The energy of the pulsed laser was 170 mJ (4.25 mJ/mm^2) with 532 nm and the full width at half maximum was about 7 ns. The bias power supply (V_{DC}) was adjustable. The current limiting resistance (R_L) was 1 MΩ, the load resistance (R_{load}) was 60.3 Ω, and the capacitance (C) was 14.4 nF. The PCSSs were tested in atmosphere at room temperature. In a single trigger test, the pulsed laser parameters were kept unchanged. The bias voltage was started at 1.0 kV and the output signals were obtained from the oscilloscope (SDS6204 H10 Pro). Then, the bias voltage was increased by 0.5 kV for each step and the test was continued until a flashover or breakdown occurred. In a multiple triggers test, the bias voltage was fixed at 3.0 kV and the frequency of the pulsed laser was 10 Hz.

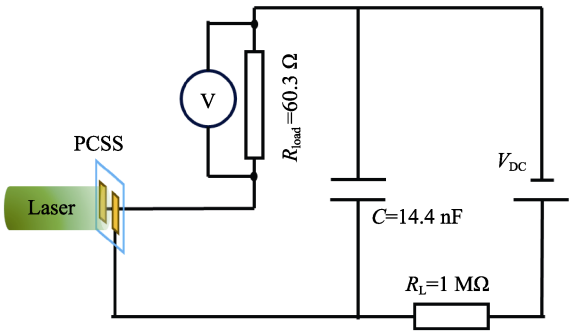

Fig. 3 Schematic diagram of PCSS testing circuit

The maximum output peak voltage across the load resistor could be read from the oscilloscope, and the input voltage was equal to bias. The minimum on-state resistance (R_{on}) of PCSS was estimated in this paper as follows:

$$R_{on} = \frac{(V_i - V_o) \times R_{load}}{V_o} \quad (1)$$

where V_i is the input voltage, V_o is the maximum output peak voltage, and R_{load} is the load resistance.

2 Results and discussion

2.1 Influence of single trigger

The impacts of FSI and BSI single trigger methods on PCSS on-state resistance were investigated. The on-state resistance of PCSS by FSI and BSI single trigger methods is presented in Fig. 4. The on-state resistance of PCSS by BSI single trigger is lower than that of PCSS by FSI single trigger at the same bias. The on-state resistances of PCSS made by SiC1 and SiC2 substrate by BSI single trigger are similar. SiC2_Ni PCSS switched 0.909 kV to 1 kV with the load resistance of 60.3 Ω by BSI single trigger and the minimum on-state resistance was 6.0 Ω. BSI single trigger method increased the effective irradiation area of the PCSS. The diameter of the laser spot was 3.6 mm, and the channel length was 3.0 mm. The substrate under two metal electrodes could be excited since the thickness of SiC substrate used in the experiments was 0.5 mm, which was less than the absorption depth of SiC at the wavelength of 532 nm. The photo-generated carrier concentration (n(t)) was higher, and total current density increased, which contributed to the decrease of PCSS on-state resistance. Besides, by BSI single trigger, a relatively lower electric field at the edge of electrodes was formed by stimulation[22]. Therefore, the PCSS damage was expected to be smaller by the BSI single trigger than that by the FSI single trigger. The microscope images of PCSSs after tests are shown in Fig. 5. The damage at the edge of electrodes was more serious, which was consistent with the theory. On this basis, the BSI single trigger method was used in subsequent tests. Fig. 4 also describes the trends of a gradual decrease in PCSS output efficiency and an increase in on-state resistance as the applied bias voltage rise. It could be the fact that carrier scattering played a dominant role at high electric field strength. The electron mobility (μ_n) is given by the following equation[14]:

$$\mu_n(E) = \frac{\mu_{n0}}{\left(1 + \left(\frac{\mu_{n0} E}{v_{sat}}\right)^{\beta}\right)^{\frac{1}{\beta}}} \quad (2)$$

where μ_{n0} is the SiC electron mobility at low electric field, v_{sat} is the SiC saturation electron drift rate, E is the applied field strength, and β is an experimentally fitted parameter. The carrier mobility decreased and the average carrier drift rate no longer increased isometrically when the external electric field became higher. As a result, the on-state resistance of PCSS increased with the rise of bias voltage.

2.2 Influence of multiple triggers

SiC1_Ni PCSS, SiC1_BGZO PCSS, SiC2_Ni PCSS, and SiC2_BGZO PCSS were used for multiple triggers

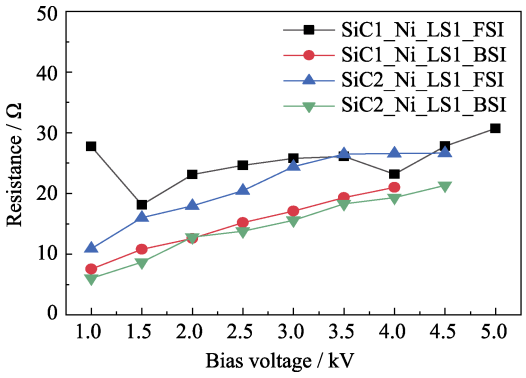

Fig. 4 Comparison of on-state resistance of SiC1_Ni and SiC2_Ni PCSS by FSI and BSI single trigger

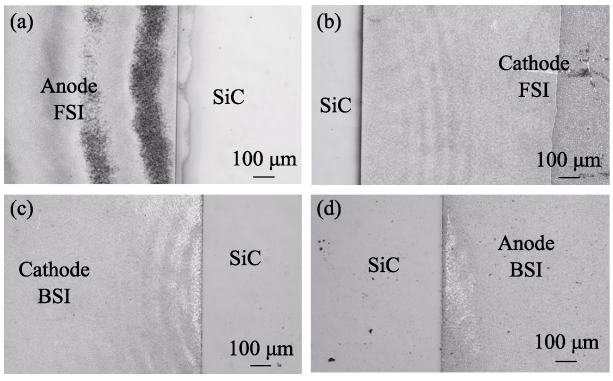

Fig. 5 Electrode damage microscope images of SiC2_Ni PCSS after FSI and BSI single trigger tests
(a) Anode FSI; (b) Cathode FSI; (c) Cathode BSI; (d) Anode BSI

tests. The output peak voltage results of PCSSs tested by a 10 Hz pulsed laser BSI single trigger at 3.0 kV bias for 200 s are shown in Fig. 6. The resistance of the BGZO films was 2.78×10^{-2} Ω·cm, and the carrier mobility was 1.78 $cm^2/(V\cdot s)$. Therefore, the on-state resistance of PCSS with BGZO films was higher than PCSS with Ni. The overall trend was that the output peak voltage of the PCSS decreased as the number of tests increased. In Fig. 6(a) and Fig. 6(c), it is noting that the SiC1_Ni PCSS and SiC1_BGZO PCSS output voltage plots were dipped and then climbed up. The reason was related to impurity elements in SiC1 and SiC2 substrates. According to the results of glow discharge mass spectrometry (GDMS) tests in Table 1, the content of aluminum (Al) elements in the SiC1 substrate (41 μg/g) was about twice as much as the content of Al element in SiC2 substrate (22 μg/g). The content of vanadium (V) elements was less than the detection limit (<0.05 μg/g) in both SiC1 and SiC2 substrates. The energy levels, which were formed by Al element, acted as hole traps. These hole traps captured carriers and released them after a longer period, inducing a rising output voltage of PCSS[23]. According to the SRH model, pulsed laser irradiation of SiC was the process of high-level injection, and the quasi-Fermi energy levels of electrons and holes moved into the conduction and valence bands, respectively. At this time, the impurity energy levels, such as Al, and the intrinsic defect energy levels tended to act as the role of recombination centers. The increase of the recombination centers in the SiC resulted in a decrease in the peak value of the output voltage of the PCSS. Besides, the carrier mobility in SiC1 was lower due to higher defect concentration. Therefore, the SiC2_Ni PCSS had a slightly higher output peak voltage than the SiC1_Ni PCSS. When the pulsed laser was off, the photogenerated carriers were recombined, and the Fermi energy levels of electrons and holes moved to the forbidden band. The Al impurity energy levels tended to act as hole traps, accumulating carriers. The Al traps released the holes during the next trigger process and contributed to the output voltage. It could be suggested that the high content of Al element in the SiC1 substrate led to an obvious climb-up tendency of PCSS output peak voltage.

The scanning electron microscope (SEM) images of SiC1_Ni PCSS and damage characterization by multiple triggers tests are shown in Fig. 7. The black branch-like ablation traces were formed at the electrodes of PCSS in Fig. 7(a, b). The energy-dispersive spectroscopy (EDS) results of the black branch-like ablation and residual metal regions in SiC1_Ni PCSS are shown in Table 2. Au, Ti, W, Ni, Si, and C elements were detected in the residual metal region. Since the detection depth was 1 μm, the atomic ratios of Au, Ni, and TiW were near 10%. In the black ablation region, low atomic ratios of the metal element compositions were detected, but the atomic ratio of the O element was up to 1.31%. On the contrary, the O element was less than the detection limit in the residual metal region. The increase of the O element indicated that

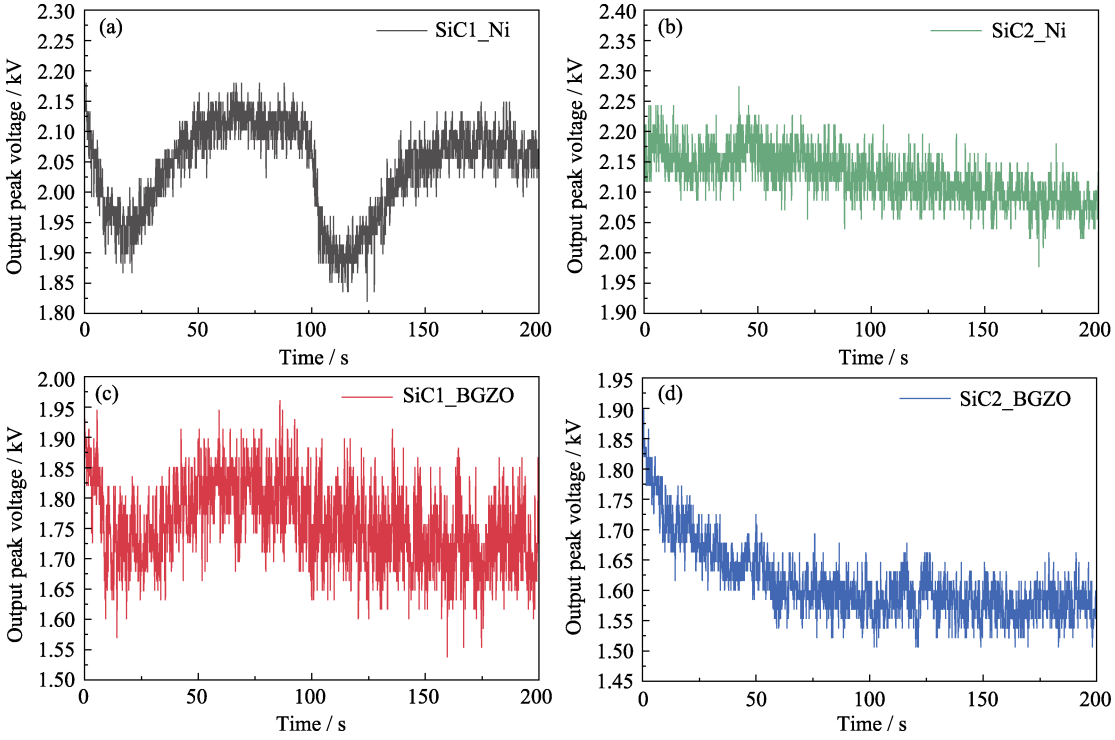

Fig. 6　Output peak voltage plots of SiC PCSSs by multiple triggers
(a) SiC1_Ni; (b) SiC2_Ni; (c) SiC1_BGZO; (d) SiC2_BGZO

Table 1 GDMS results of SiC1 and SiC2

Element	SiC1/(μg·g^{-1})	SiC2/(μg·g^{-1})
B	3.2	3.0
Al	41	22
V	<0.05	<0.05

thermal oxidation occurred in the black ablation region. When the PCSS was triggered, the photogenerated carriers were accelerated toward the electrode edge and formed hot carriers at a high electric field. The impact ionization effect was more dramatic due to the greater electric field strength at the edge of the PCSS electrode. When the trigger times were few, the damage was not obvious. With more trigger times, metals were oxidized or melted owing to the high PCSS temperature. The electron avalanche effect played an important role in the damage of electrodes and a large number of long sequences of phonons accumulated due to the free mobile carriers[15]. The thermal effect caused by phonons decreased the capture rate of the carrier. The temperature rose until cracks happened and black ablation occurred. Consequently, the material in these regions reacted with oxygen in the air. The black traces extended since the high electric strength region formed near the high-resistance traces, which was similar to the edge of electrodes. The stimulation indicated that the electric field strength at the edge of the anode was higher than at the edge of the cathode when PCSS was turned on[17]. Besides, there was the order of magnitude difference between electron mobility (800–1000 cm^2/(V·s)) and hole mobility (~40 cm^2/(V·s)) of SiC. Therefore, the thermal stress was higher at the edge of the anode due to a more serious electron avalanche effect.

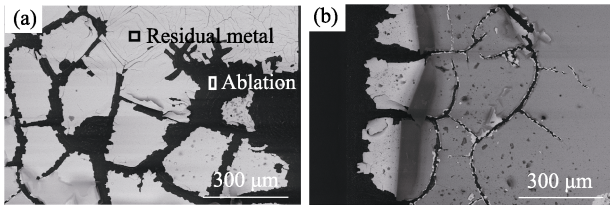

Fig. 7 SEM images of SiC1_Ni PCSS damage after multiple triggers tests
(a) Cathode; (b) Anode

Table 2 EDS results of SiC1_Ni PCSS

Element	Residual metal/% (in atom)	Ablation/% (in atom)
C	53.41	55.91
O	BDL	1.31
Si	13.85	42.42
Ti	2.03	BDL
Ni	11.14	0.25
W	7.41	BDL
Au	12.17	0.10

BDL: Below detection limit of the EDS

Fig. 8(a, b) are electrode damage images of SiC1_BGZO PCSS after a single trigger test for comparison and Fig. 8 (c, d) are images after multiple triggers tests. No significant black ablation damage was on the PCSS indicating that the BGZO films served to homogenize the electric field. The concentric ablation traces occurred at the anode of SiC1_BGZO PCSS in Fig. 8(d). The nodular-like damage, which was circled in Fig. 8(d), was also observed at the anode. The morphology was similar to the damage of AZO films on PCSS[20]. The damage was related to the thermal shock effect caused by the pulsed laser. However, the regular concentric damage in this work was few reported. It might be explained by both the laser diffraction and the thermal effect caused by carriers. It has been reported that the diffraction of the pulsed laser caused a concentric pattern in C/SiC material, especially when the energy of the laser was high[24]. Nevertheless, there was no concentric damage on the cathode of SiC1_BGZO PCSS in Fig. 8(c). The reasons for the damage could be explained as follows. On the one band, a large amount of carrier was generated in the concentric region due to the laser diffraction at the electrodes of PCSS. On the other hand, the carrier tended to transport in the low-resistance channel at the applied bias voltage. In addition, the circumferential thermal stress was formed under these conditions. The metals on the electrodes fell off and BGZO films ablated due to the thermal stress, which was similar to the situation in SiC1_Ni PCSS. The temperature became higher as the accumulation of thermal effect and the concentric damage became more serious during the multiple triggers. Nevertheless, there was no concentric damage on the cathode of SiC1_BGZO PCSS. The holes at the cathode were easier to recombine since the BGZO film was a heavy n-doped material. As a result, the cathode was damaged owing to the heating effect in multiple triggers tests.

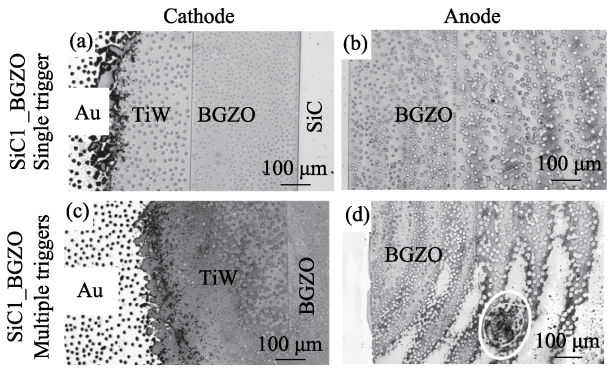

Fig. 8 Microscope images on electrode damage of SiC1_BGZO PCSS after trigger tests
(a) Cathode and (b) anode after a single trigger test; (c) Cathode and (d) anode after multiple triggers

The degree of concentric damage became more serious at the inner of the anode rather than at the edge in Fig. 8(d). The high electric field strength was also formed at the border of the laser spot by the BSI single trigger method. The unirradiated region was a high-resistance state while the irradiated region was a low-resistance state. For a similar situation of the FSI single trigger method at the edge of electrodes, black ablation traces tended to expand at the border of the spot laser SiC1_Ni PCSS. The black ablation traces were arc-like. The high electric field at the border of the laser spot caused damage due to circumferential thermal stress caused by the laser. It could be concluded that the effect of laser diffraction and thermal stress predominated in SiC1_BGZO PCSS and had a synergy of damage in SiC1_Ni PCSS. The detailed reasons for the concentric traces and causes of laser diffraction need further study.

In SiC2_BGZO PCSS, the BGZO films fell off and ablated due to thermal stress. The adhesion between the metal and the BGZO films was poor since they were separately sputtered. Besides, more defects and bubbles occurred in BGZO films after tests because the quality of BGZO films was susceptible to decomposition when the temperature was higher than 800 ℃[25]. Therefore, the on-state resistance of PCSS with BGZO films on SiC1 was lower than PCSS with BGZO films on SiC2.

3 Conclusions

Various lateral PCSSs were prepared on HPSI 4H-SiC substrates. Tests were done for different trigger methods and electrodes component PCSSs. The PCSS with Au/TiW/Ni electrode components on SiC2 substrate triggered by a 532 nm, 170 mJ laser with BSI single trigger had a minimum on-state resistance of 6.0 Ω at 1 kV bias voltage. The on-state resistance and damage of PCSS can be reduced by the BSI single trigger when the diameter of the laser spot is larger than the PCSS channel length. In multiple triggers tests, the output peak voltage of PCSS increases due to Al hole traps in the SiC substate. Both the edge of the electrodes of PCSS and the border of the laser spot are easier to damage. The black branch-like damage in PCSS with Au/TiW/Ni components is mainly caused by thermal stress, which was related to the hot carrier effect. The concentric damage at the anode of PCSS with Au/TiW/BGZO components is mainly caused by the laser diffraction effect and thermal effect owing to carrier transportation. In the future, the formation process and mechanism of concentric damage, which is less reported in SiC PCSS, will be further investigated. The BGZO films can be prepared by chemical vapor deposition and the design of PCSS will be modified according to the damage.

References:

[1] CHANG S H, LIU X C, HUANG W, *et al*. Preparation and properties of lateral contact structure SiC photoconductive semiconductor switches. *Journal of Inorganic Materials*, 2012, **27(10):** 1058.

[2] BRAGG J W, SULLIVAN W W, MAUCH D, *et al*. All solid-state high power microwave source with high repetition frequency. *Review of Scientific Instrument*s, 2013, **84(5):** 054703.

[3] HARRIS J R, BLACKFIELD D, CAPORASO G J, *et al*. Vacuum insulator development for the dielectric wall accelerator. *Journal of Applied Physics*, 2008, **104(2):** 023301.

[4] ZHANG D, XU Z, CHENG G, *et al.* Strongly enhanced THz generation enabled by a graphene hot-carrier fast lane. *Nature Communications*, 2022, **13:** 6404.

[5] YAN C F, SHI E W, CHEN Z Z, *et al*. Super fast and high power SiC photoconductive semiconductor switches. *Journal of Inorganic Materials*, 2008, **23(3):** 425.

[6] MAJDA-ZDANCEWICZ E, SUPRONIUK M, PAWŁOWSKI M, *et al.* Current state of photoconductive semiconductor switch engineering. *Opto-Electronics Review*, 2018, **26(2):** 92.

[7] CHOWDHURY A R, NESS R, JOSHI R P. Assessing lock-on physics in semi-insulating GaAs and InP photoconductive switches triggered by subbandgap excitation. *IEEE Transactions on Electron Devices*, 2018, **65(9):** 3922.

[8] XU M, WANG Y, LIU C, *et al.* Photoexcited carrier dynamics in a GaAs photoconductive switch under nJ excitation. *Plasma Science and Technology*, 2022, **24(7):** 075503.

[9] JAMES C, HETTLER C, DICKENS J. Design and evaluation of a compact silicon carbide photoconductive semiconductor switch. *IEEE Transactions on Electron Devices*, 2011, **58(2):** 508.

[10] YANG F, WANG Z, LIANG Z, *et al.* Electrical performance advancement in SiC power module package design with kelvin drain connection and low parasitic inductance. *IEEE Journal of Emerging and Selected Topics in Power Electronics*, 2019, **7(1):** 84.

[11] CHU X, LIU J, XUN T, *et al*. MHz repetition frequency, hundreds kilowatt, and sub-nanosecond agile pulse generation based on linear 4H-SiC photoconductive semiconductor. *IEEE Transactions on Electron Devices*, 2022, **69(2):** 597.

[12] SULLIVAN J S, STANLEY J R. 6H-SiC photoconductive switches triggered at below bandgap wavelengths. *IEEE Transactions on Dielectrics and Electrical Insulation*, 2007, **14(4):** 980.

[13] HETTLER C, SULLIVAN W W, DICKENS J, *et al.* Performance and optimization of a 50 kV silicon carbide photoconductive semiconductor switch for pulsed power applications. Proceedings of the 2012 IEEE International Power Modulator and High Voltage Conference, San Diego, 2012.

[14] HUANG J, HU L, MA Z, *et al*. Study on photoelectric efficiency and failure mechanism of high purity 4H-SiC PCSS. *IEEE Transactions on Electron Devices*, 2023, **70(11):** 5762.

[15] ZHU K, DOGAN S, MOON Y T, *et al*. Effect of n^+-GaN subcontact layer on 4H-SiC high-power photoconductive switch. *Applied Physics Letters*, 2005, **86(26):** 261108.

[16] XIAO L, YANG X, DUAN P, *et al*. Effect of electron avalanche break-down on a high-purity semi-insulating 4H-SiC photoconductive semiconductor switch under intrinsic absorption. *Applied Optics*, 2018, **57(11):** 2804.

[17] MAUCH D, SULLIVAN W, BULLICK A, *et al.* High power lateral silicon carbide photoconductive semiconductor switches and investigation of degradation mechanisms. *IEEE Transactions*

on Plasma Science, 2015, **43(6):** 2021.
[18] ZHENG Z, HUANG W, HAN W W, *et al*. Analyzing the effects of aluminum-doped ZnO and Ag layers for the transparent electrode vertical PCSS. *IEEE Transactions on Electron Devices*, 2020, **67(6):** 2414.
[19] ZHOU T Y, LIU X C, HUANG W, *et al*. Application of an Al-doped zinc oxide subcontact layer on vanadium-compensated 6H–SiC photoconductive switches. *Chinese Physics B*, 2015, **24(4):** 044209.
[20] WANG B, WANG L, NIU X, *et al*. Breakdown behavior of SiC photoconductive switch with transparent electrode. *AIP Advances*, 2022, **12(8):** 085210.
[21] CHOWDHURY A R, MAUCH D, JOSHI R P, *et al*. Contact extensions over a high-k dielectric layer for surface field mitigation in high power 4H-SiC photoconductive switches. *IEEE Transactions on Electron Devices*, 2016, **63(8):** 1.
[22] FENG Z, LUAN C, XIAO L, *et al*. Performance of a novel rear-triggered 4H-SiC photoconductive semiconductor switch. *IEEE Transactions on Electron Devices*, 2023, **70(2):** 627.
[23] FU W, WANG L, WANG B, *et al*. Investigation on the photocurrent tail of vanadium-compensated 4H–SiC for microwave application. *AIP Advances*, 2022, **12(9):** 095121.
[24] ZHAI Z, ZHANG R, TANG A, *et al*. Fabrication of microstructure on C/SiC surface *via* femtosecond laser diffraction. *Materials Letters*, 2021, **293:** 293711
[25] KIM I W, DOH S J, KIM C C, *et al*. Effect of evaporation on surface morphology of epitaxial ZnO films during postdeposition annealing. *Applied Surface Science*, 2005, **241(1):** 179.

非本征背照触发平面型 4H-SiC 光导开关性能研究

王 浩[1,2], 刘学超[1], 郑 重[3], 潘秀红[1], 徐锦涛[1], 朱新锋[1,2],
陈 锟[1], 邓伟杰[1], 汤美波[1], 郭 辉[3], 高 攀[4]

(1. 中国科学院 上海硅酸盐研究所, 上海 201889; 2. 中国科学院大学, 北京 100049; 3. 西安电子科技大学 微电子学院, 西安 710071; 4. 上海电机学院 材料学院, 上海 201306)

摘 要: 光导开关(PCSS)是脉冲高功率系统和微波技术应用中的关键器件, 减小碳化硅(SiC)光导开关的损伤, 延长器件寿命是重要的研究方向。本工作在直径 4 英寸、厚度 500 μm 的高纯半绝缘 4H-SiC 衬底上制备多种结构的光导开关器件, 重点研究了导通电阻和损伤机制。1 kV 偏压下, 采用 532 nm、170 mJ 的脉冲激光背面照射触发经过 950 ℃退火的 Au/TiW/Ni 电极体系的碳化硅光导开关, 最小导通电阻为 6.0 Ω。当激光光斑直径大于光导开关器件沟道宽度时, 采用背面照射触发相较于前面照射触发可以减小导通电阻并减轻损伤。碳化硅光导开关器件在 10 Hz 激光下触发 200 s, Au/TiW/Ni 体系光导开关产生黑色枝状烧蚀损伤, 主要原因是热载流子引起的热应力。采用 400 ℃退火的硼镓共掺杂氧化锌(BGZO)薄膜替换金属 Ni, 黑色烧蚀得到缓解, 但是在光导开关阳极出现同心圆弧损伤, 其主要成因是脉冲激光的衍射和热效应的共同作用。

关 键 词: 碳化硅; 光导开关; 导通电阻; 失效分析

中图分类号: TN36 **文献标志码:** A **文章编号:** 1000-324X(2024)09-1070-07